Pharm Res (2013) 30:424–434
DOI 10.1007/s11095-012-0884-4

RESEARCH PAPER

Rapid Lymph Accumulation of Polystyrene Nanoparticles Following Pulmonary Administration

Abdul Khader Mohammad • Lenah K. Amayreh • John M. Mazzara • Joshua J. Reineke

Received: 4 May 2012 / Accepted: 5 September 2012 / Published online: 20 September 2012

ABSTRACT

Purpose Pulmonary administration of polymeric nanoparticle drug delivery systems is of great interest for both systemic and local therapies. However, little is understood about the relationship of particle size and pulmonary absorption. We investigated uptake and biodistribution of polystyrene nanoparticles (PN) of 50 nm, 100 nm, 250 nm, and 900 nm diameters in mice following administration to lungs via pharyngeal aspiration.

Methods The amount of PN in tissues was analyzed by gel permeation chromatography (GPC).

Results At 1 h, larger diameter PN (250 nm and 900 nm) had the highest total uptake at around 15% of administered dose, whereas the smaller diameter PN (50 nm and 100 nm) had uptake of only 5–6%. However, at 3 h, the 50 nm PN had the highest total uptake at 24.4%. For each size tested, the highest nanoparticle deposition was observed in the lymph nodes (LN) as compared to other tissues accounting for a total of about 35–50% of absorbed nanoparticles.

Conclusion PN size impacts the rate and extent of uptake from lungs and, further, the extent of LN deposition. The extent of uptake and lymph distribution of the model, non-degradable PN lends potential to pulmonary administered, biodegradable polymeric nanoparticles for delivery of therapeutics to regional lymph nodes.

Electronic supplementary material The online version of this article (doi:10.1007/s11095-012-0884-4) contains supplementary material, which is available to authorized users.

A. K. Mohammad • L. K. Amayreh • J. M. Mazzara • J. J. Reineke
Department of Pharmaceutical Sciences
Eugene Applebaum College of Pharmacy & Health Sciences
Wayne State University
Detroit, Michigan 48201, USA

J. J. Reineke (✉)
Wayne State University
Room 3136, Eugene Applebaum Building, 259 Mack Avenue
Detroit, Michigan 48201, USA
e-mail: reineke@wayne.edu

KEY WORDS biodistribution · lymph node · pharyngeal aspiration · polystyrene nanoparticle · pulmonary delivery

ABBREVIATIONS

ALN	axillary lymph nodes
BAL	bronchoalveolar lavage
BLN	brachial lymph nodes
CLN	cervical lymph nodes
DLS	dynamic light scattering
GPC	gel permeation chromatography
H&E	hematoxylin and eosin
LN	lymph node(s)
PN	polystyrene nanoparticles
RES	reticuloendothelial system
RI	refractive index
TEM	transmission electron microscopy

INTRODUCTION

The lungs possess many advantages as an administration pathway including an alveolar surface area of around 100 m^2 (1), high solute permeability, limited proteolytic activity (2), a very thin alveolar epithelium of 0.2 μm, and extensive vasculature (3). Considerable research has been carried out in investigating and improving the pharmacokinetics of several drugs, peptides and proteins from the lungs (4–8). In the field of pulmonary drug delivery, nanoparticles have gained increasing attention as they may provide targeted delivery, sustained release, reduced dosage frequency, and improved patient compliance (3). Recently, it has been shown that nanoparticles with a maximum diameter of up to 34 nm are absorbed into the blood stream and are also translocated to the regional lymph nodes after administration to lungs (9). However, the size range investigated may be below that of particles that would be well suited for many

drug delivery applications (such as polymeric nanoparticles). Therefore, considering the potential of lungs for the purpose of local and systemic drug delivery, we investigated the translocation and organ distribution of relatively larger nanoparticles through the pulmonary route. To test this, the biodistribution and uptake characteristics of polystyrene nanoparticles (PN) of mean diameters 50 nm, 100 nm, 250 nm, and 900 nm in mice, following administration to lungs by pharyngeal aspiration, were evaluated. Polystyrene nanoparticles were used as a convenient non-degradable model system due to their high degree of monodispersity; a prime importance when evaluating the effect of particle size on biodistribution. Since PN are non-degradable, they can be used to quantitatively track the fate of PN administered *in vivo*. Delineation of the relationship of PN size to pulmonary translocation and fate *in vivo* will influence the development of degradable systems of similar physicochemical properties for applications to and through the lung.

It has been shown that PN in the range of 250 nm–3 μm present an optimal size for phagocytosis, whereas, those less than 250 nm were shown to be phagocytosed less efficiently (10). Additionally, particles less than 200 nm in size are extensively internalized via clathrin mediated endocytosis (11). Therefore, nanoparticle mean diameters in this study were selected based on the premise that different uptake mechanisms may possibly lead to varied biodistribution profiles. The main objective of this study was to understand the effect of nanoparticle size on their uptake and biodistribution from lungs, specifically investigating the lymph deposition. Here, with a gel permeation chromatography (GPC)-based detection technique, yielding the quantitative concentration of polystyrene present in each tissue from tissue extracts, we determine the pulmonary uptake potential and biodistribution of PN.

MATERIALS AND METHODS

Materials

PN of mean diameters 50 nm, 100 nm, 250 nm, and 900 nm were purchased from Polysciences Inc. and characterized. Nanoparticle suspensions of 1% *w/v* concentration were used for all experiments and were characterized as described in Supplementary Materials. Hematoxylin, eosin Y disodium salt, ethyl alcohol (anhydrous), xylene (histological grade), and Permount® were purchased from Fisher Scientific. Solvents were of HPLC grade or higher, and were purchased from Fisher Scientific.

Animals

Male BALB/c mice weighing between 20–25 g (Charles River Inc.) were used following acclimation for one week. Food and water were available to the animals *ad libitum*. All animal procedures adhere to American Veterinarian Medical Association (AVMA) Guidelines, Wayne State University Institutional Animal Care and Use Committee (IACUC) approval, in accordance with the Office of Laboratory Animal Welfare (OLAW) Public Health Service Policy on Humane Care and Use of Laboratory Animals, and Principals of Laboratory Animal Care. All studies were performed in animal cohort groups of 6 (n=6).

Methods

Administration of Nanoparticles to Mice

Mice were anaesthetized by inhalation of 2.5% *v/v* isoflurane and placed on a slant board with the back resting on the board, and partially suspended with a rubber band by their incisors. The tongue was held gently in extension and a PN suspension was placed in the pharynx region using a Hamilton microliter syringe with a 22s gauge needle. The tongue was continuously held in extension until several breaths had elapsed. Once the entire dosage (150 μl) had been administered, the mice were returned to their housing and laid on their side. This method has been validated in comparison to intratracheal administration and allows for greater lung deposition and higher dose-to-dose consistency (12). To ensure that our results are not dependant on the administration method we compared pharyngeal aspiration and intratracheal instillation for a single study group. Nanoparticle suspensions were used as provided from Polysciences Inc. (1% *w/v* suspension). However, additional biodistribution studies were performed with washed nanoparticles suspended in normal saline by sonication. Particle suspensions following the wash were sized with dynamic light scattering (DLS) on a 90Plus Particle Size Analyzer (Brookhaven Instrument Corporation) and compared to the commercially available suspensions. There was no significant difference in the size characterizations of the two suspensions (Table I).

Harvesting of Tissues from Mice

After the administration of nanoparticles, at predetermined intervals of 1, 3, and 5 h, various tissues were harvested.

Table I Size of Polystyrene Nanoparticles Before and After Washing with Deionized Water

Parameters	Before washing	After washing
Size[a] (nm)	833.3 ± 31	788.2 ± 89
PDI	0.102 ± 0.039	0.052 ± 0.03

[a] The original nanoparticle suspension, 10 mg/ml concentration, was diluted to a concentration of 0.1 mg/ml for sizing and washed particles were sized at the same concentration

Before performing the terminal surgery, the mice were anesthetized by inhalation of 5% *v/v* isoflurane. The list of tissues harvested is as follows: axillary lymph nodes (ALN), brachial lymph nodes (BLN), mesenteric lymph node (MLN), cervical lymph nodes (CLN), lungs, liver, stomach, small intestine, kidneys, spleen, blood, brain, heart, bronchoalveolar lavage (BAL), and thymus. For collecting the BAL, 0.5 ml of normal saline was injected into the lungs *per os* and the inflated lungs were gently massaged and the rinsate was collected back into the syringe.

Tissue Processing

Tissue samples were processed and analyzed by a method modified from previously described studies (13,14). The harvested tissues were physically homogenized using a tissue homogenizer. Following homogenization, the tissues were frozen and lyophilized to remove water. To each lyophilized tissue vial, chloroform was added and placed on a mixer for extraction over 96 h. Following this, all the tissues were filtered using a 0.2 μm PTFE Millipore filter. The filtrate containing the polymer/tissue extracts was frozen at −80°C overnight and lyophilized. Following this, the polymer and/or tissue extracts remain in the vial. To each vial, a known volume (0.5 ml or 1 ml) of tetrahydrofuran was added, placed on the mixer for 1 h and then filtered into a conical GPC analysis vial using a 0.2 μm syringe filter. To verify this method of extraction for PN, three tissues (ALN, heart, spleen) were doped with a known amount of PN and processed to extract PN as mentioned above. Upon analysis by GPC, as described in "Method of Analysis" section, the extraction yield for PN for the three tissues was 94.5, 98.2, and 90.9% (Table II).

Method of Analysis

Analysis of polymer concentration from tissue extracts was performed by GPC (GPC Max VE 2001, Viscotek Corporation) equipped with a column bank consisting of three columns with size exclusion limits of 4 million, 70,000, and 5,000 Da. A refractive index (RI) detector (VE 3580, Viscotek Corporation) was used for polystyrene detection. The area under the polystyrene peak was compared to a standard curve of GPC peaks for polystyrene samples of known concentration. This method yields absolute quantitative data and is label-free. The amount of polymer in each tissue is expressed as a percent of administered dose. As this is a quantitative method, mass balance was analyzed for all study groups (Supplementary Material Figure S2) and the quantity of PN residing in the lung tissue at each time point is presented (Supplementary Material Figure S3).

Table II Recovery of PN from Doped Tissues After Processing

Tissue	Amount of PN added (mg)[a]	Amount recovered (mg)	% Recovery
ALN	0.55	0.52	94.5
Heart	0.55	0.54	98.2
Spleen	0.55	0.50	90.9

[a] To each of the tissues, 0.55 mg of PN was added and the tissues were subjected to the processing steps as described. After processing, each of these tissues were analyzed for the amount of PN recovered after processing

Tissue Histology

Five hours after administering the particles by pharyngeal aspiration, the mice were sacrificed and the harvested tissues (lungs and lymph nodes) were fixed with 4% paraformaldehyde overnight at 4°C. The lung sections were cryosectioned on a cryotome (Cryotome FSE, Thermo Scientific) into 10 μm-thick sections, which were then stained with standard hematoxylin and eosin (H&E) staining (Harris hematoxylin for 3 min followed by running tap water for 1 min, eosin Y for 5 min, 70% ethanol for 1 min, 95% ethanol for 1 min, 100% ethanol for 1 min, two rinses in 100% Xylene for 1 min each) and cover slip mounted. The stained lung and lymph node tissues were then observed under inverted bright field microscopy (Olympus 1×71, DP70).

Transmission Electron Microscopy

Portions of tissues harvested for histology were also collected for transmission electron microscopy (TEM). Tissues were dissected down to 1–2 cubic millimeters and fixed in 2% paraformaldeyde, 1.25% glutaraldehyde, 0.2% sucrose and 25 mM HEPES buffer in 0.12 M sodium cacodylate TEM buffer at 4°C for 4 h. Tissues were then washed in 0.12 M sodium cacodylate, gradually going to room temperature. A secondary fix in 3% glutaraldehyde and 4% tannic acid (lipid mordant) in sodium cacodylate at 37°C for 1 h, was performed and rinsed with 0.12 M sodium cacodylate. Osmium tetroxide and 2% sodium cacodylate were used as post-fixative stains. For application of a non electron-dense staining, samples were stained *en block* with 2% uranyl acetate followed by dehydrating tissues in graded ethanol series of 10 min each. Fixed tissues were transfer to conical Beem capsules (Electron Microscopy Sciences; Hatfield, PA). Propylene oxide was added quickly and enclosed with the tissue for 2 h. Finally, Embed 812 was added in gradual ratios for 2 h. Samples were cured at 55°C for 2 or 3 days. Tissues were ultrathin sectioned using a microtome Diatome with a diamond knife, transferred to Formvar film copper grids, and post-stained with NaOH-treated 0.03% lead citrate for 5 min. The stained tissues were then observed under a Zeiss EM-900 TEM at 50 Kv.

Statistical Analysis

Data are expressed as mean ± SEM with cohort sizes of 6. Statistical analysis was performed using one-way ANOVA followed up by Tukey's test with OriginPro® software. The differences were defined statistically significant at $p<0.05$.

RESULTS

The mean particle diameter, zeta potential, and surface morphology for all PN formulations were analyzed as described in Supplementary Materials. All particles were found to have a high degree of monodispersity around their respective mean diameters, negative zeta potential, and smooth surface morphology.

Effect of Size on the Total Uptake of PN

Total uptake for all PN sizes at 1, 3 and 5 h is shown in Fig. 1. At 1 h, the total uptake for 50 nm (5.2%) and 100 nm (6.2%) PN is low, but is higher for 250 nm and 900 nm at 14.8% and 14.7%, respectively. At the 3 h time point, we see a reversal in trend where the 50 nm PN has the highest total uptake (24.4%) and an increase in PN size leads to a decrease in total uptake. At this time point, the total uptake for 100 nm is 11.3% and for 250 nm is 13.1%, further decreasing to 4.8% for the 900 nm PN. A similar trend can be seen at the 5-hour time point where the highest total uptake is for 50 nm PN at 20.9% and the lowest is for 900 nm PN at 7.5%. At this time point, the total uptake for 100 nm and 250 nm PN is 15.3% and 12.4%, respectively. Inset in Fig. 1 is a representative histology image of the lung 5 h after 50 nm PN administration. It can be noted that there is minimal infiltration and alveoli are intact. While it is not possible to see discrete particles at the image

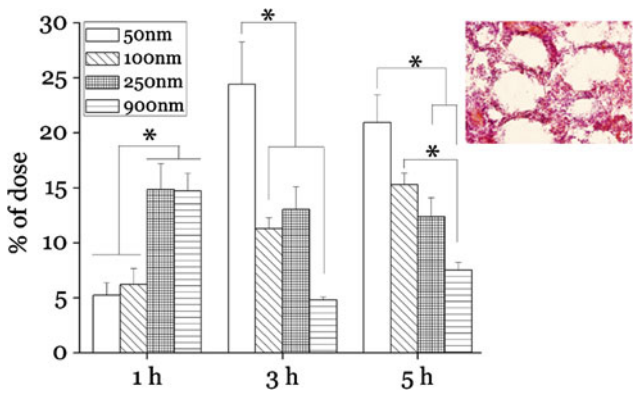

Fig. 1 Extrapulmonary uptake of 50, 100, 250 and 900 nm PN at 1, 3 and 5 h following pulmonary administration as a % of dose. *$p<0.05$ ($n=6$; mean ± SEM). Inset; histology of lungs after administration of 50 nm PN (630X magnification).

magnification, no aggregated clusters of nanoparticles were seen either. When the lung tissue was further investigated with TEM, discrete PN are seen without the presence of aggregates (Fig. 2). Both larger PN and small PN (representative images for 900 nm and 50 nm PN shown in Fig. 2) were internalized from the alveolar space into the interalveolar septum without observed disruption to the epithelial cell layer.

Effect of Size on the Biodistribution of PN

The biodistribution of PN of different sizes (50 nm, 100 nm, 250 nm, and 900 nm) at time points of 1, 3, and 5 h is presented in Figs. 3, 4, and 5. The distribution of PN in tissues is represented as % of the total administered dose. In this study, the amount of PN in lymph nodes (LN) is the cumulative amount of PN detected in each of the tissues including axillary, brachial, cervical, mesenteric lymph nodes, and thymus (a primary lymphoid organ). The highest deposition of nanoparticles was in the lymph nodes and the lymph node of highest deposition was the axillary node for each of the sizes studied. LN deposition is discussed in further detail in the subsequent section.

In the liver, the primary reticuloendothelial system (RES) organ, there is minimal presence of PN across all time points and sizes. The highest level of liver accumulation is 1.1% of the dose for 50 nm at hour 3. For all sizes, no PN were detected in the liver at 1 h post-administration. Further, the larger 900 nm PN were not found in the liver during any of the time points tested.

In the first hour after pulmonary administration the only organ to have significant accumulation outside of the LN is the spleen. In spleen at 1 h, we see a general trend of increasing PN accumulation with an increase in size, the highest being 2.2% for 900 nm PN. Distribution to all other tissue compartments was minimal (<1%) including the central blood compartment.

However, by hours 3 and 5 post-pulmonary administration, a significant amount of 50 nm PN (3.4% and 3.1%, respectively) was detected in the blood compartment. Blood distribution was low for all other sizes with the highest being 1.3%. At these time points, PN distribution was highest in the LN followed by heart and spleen, with very low amounts detected in other tissues. This was true for all sizes except for 50 nm where more PN were present in the blood than spleen. There is also a general inverse relationship to PN size across all tissues with smaller PN having higher deposition than larger PN.

To ensure that the uptake and biodistribution results reported here were not an artifact of the nanoparticle suspension media, we tested 900 nm PN after a series of washes and re-suspension in sterile saline. Sizing data for the two suspensions can be found in Table I. The uptake and LN

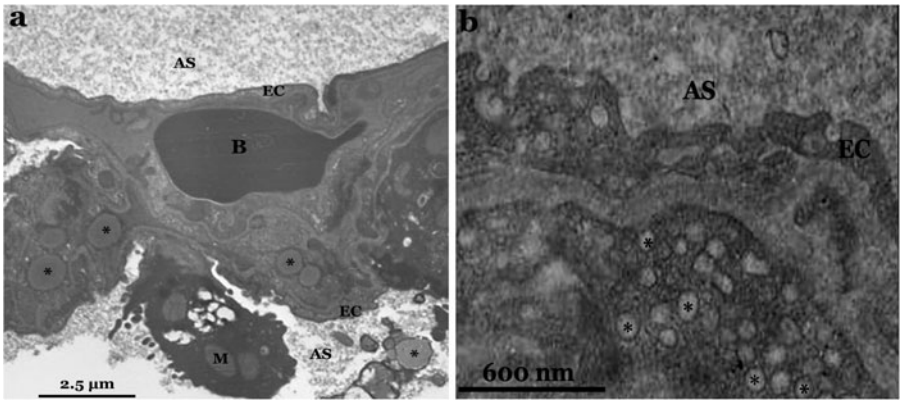

Fig. 2 TEM images of lungs after 900 nm (**a**) and 50 nm (**b**) PN administration. AS, alveolar space; B, red blood cell; EC, epithelial cell layer; M, mitochondria; *, PN. Scale bars are 2.5 μm (**a**) and 600 nm (**b**).

distribution of the washed nanoparticles (biodistribution shown in Fig. 6) were similar to the manufacturer suspension without statistical differences. However, the washed particles did have significantly less distribution to the heart and spleen. Additionally, for a single study group (50 nm at 5 h), intratracheal installation was compared to pharyngeal aspiration to identify any possible dependencies of our results on the method of administration. Comparison of the biodistribution following the two methods is shown in Fig. 7. The pattern of tissue distribution remained the same with the LN having the highest deposition; however, both the uptake and the LN distribution were significantly less for the intratracheal administration as discussed in further detail in "Discussion" section.

Lymph Distribution of PN

PN were deposited in greater amounts in the lymph nodes as compared to other tissues for all PN sizes and time points as can be seen in Figs. 3, 4, and 5. The amount of PN deposited in the lymph nodes was highest for 50 nm size at 5 h (12.3% of dose). The 100 nm PN show a trend of increasing lymph deposition with time ranging from 3.6% to 6.9% over the period of 5 h. For the 250 nm size, there is no statistically significant difference in the amount of PN deposited in the lymph nodes at the three time points where the amount of lymph deposition of PN ranges from 6.5 to 8.0% of dose. For the 900 nm PN, the lymph deposition is the highest at 1 hour (6.2%). Similar to the results of total PN uptake, the PN distribution to the lymph is highest for the larger PN in the first hour, but for 3 and 5 h the trend reverses resulting in an inverse relationship with size (smaller PN have highest LN distribution).

However, when the lymphatic distribution of PN is normalized for the amount of PN uptake (i.e. the amount of PN in the lymph nodes calculated as a percentage of the total absorbed PN from the lungs) further information on LN specificity and PN size relationship is gained. From the normalized lymphatic distribution (Fig. 8), the 1 h time point displays a general decrease in the percentage of absorbed PN depositing in LN with increase in PN size; though no statistical differences exist. However, at the 3-hour time point we see a general trend of increasing percentage of absorbed PN depositing in lymph nodes for each increase in PN size with no statistical significance at this time point. Furthermore, at this time point the 900 nm PN has a

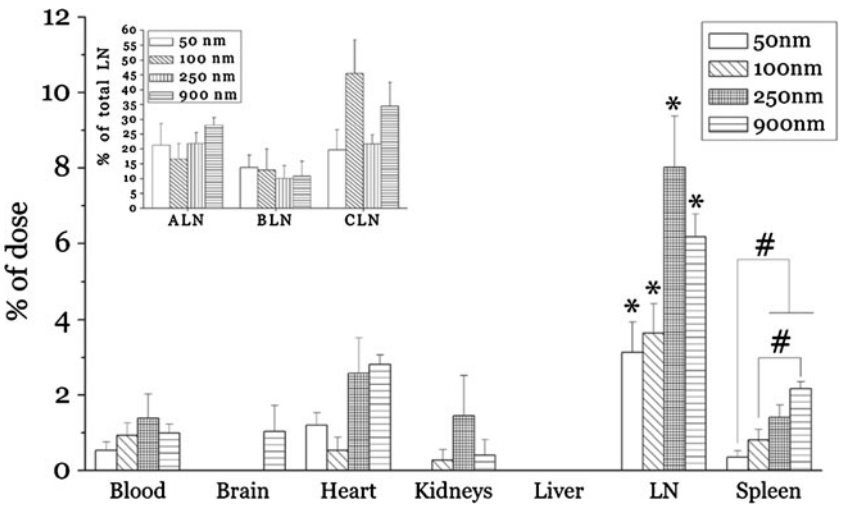

Fig. 3 PN biodistribution 1-hour after pulmonary administration as a % of dose. LN, Lymph nodes; *, $p < 0.05$ when compared to every tissue among each size; #, $p < 0.05$ when comparing the two tissues represented by this symbol ($n=6$; mean ± SEM). Inset; percent PN distribution among various LN. ALN, axillary lymph nodes; BLN, brachial lymph nodes; CLN, cervical lymph nodes.

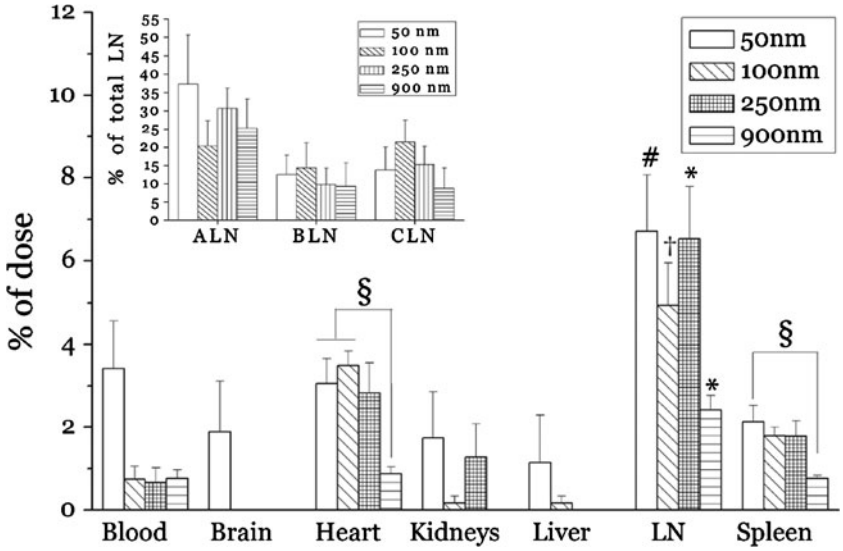

Fig. 4 PN biodistribution 3-hours after pulmonary administration as a % of dose. LN-Lymph nodes; *, $p < 0.05$ when compared to every tissue among each size; †, $p < 0.05$ when compared to every tissue except for heart, #, $p < 0.05$ when compared to every tissue except for heart and blood. §, $p < 0.05$ between the two tissues represented by this symbol ($n=6$; mean ± SEM). Inset; percent PN distribution among various LN. ALN, axillary lymph nodes; BLN, brachial lymph nodes; CLN, cervical lymph nodes.

normalized lymph deposition of 50.3% compared to 33.4% for the 50 nm PN. The 5 h normalized LN distribution reveals that no trend and no significant differences exist among all NP sizes.

To further investigate the LN specificity beyond the normalized data, the amount of PN per gram of tissue was plotted (Fig. 9) based on the wet tissue weight directly following tissue harvesting. For 50 nm PN at 5 h, the amount of PN per gram of tissue in LN (3 mg/g) is more than 4-fold higher as compared to that in spleen (0.7 mg/g), which is the organ with the next highest distribution of 50 nm PN. Similarly, the amount of PN per gram of tissue in LN when compared to liver and spleen combined together is 3 times higher for 100 nm, more than 4 times higher for 250 nm, and ~4 times higher for 900 nm PN (Fig. 9). Similar results are observed at the 1 h and 3 h time points where the amount of PN deposition in LN is multiple fold higher as compared to the liver and spleen (Fig. 9).

Since the ALN was the tissue of highest PN distribution among the lymph nodes tested, ALN tissue was histologically examined and a representative image of ALN with 250 nm PN is shown (Fig. 10). It can be seen that a cluster of PN is present in the ALN. The PN cluster is an irregularly shaped aggregate distinct from that of the relatively larger, and round nuclei of the ALN. The PN cluster becomes obvious in the magnified image inset in Fig. 10.

DISCUSSION

Pulmonary absorption of nanoparticles has been investigated by several research groups; however, most of the previous work consider non-polymeric nanoparticles (i.e. inorganic nanoparticles, carbon nanotubes, and environmental pollutants) of very small size, less than 30 nm diameter, which are not conducive for many drug delivery applications. In

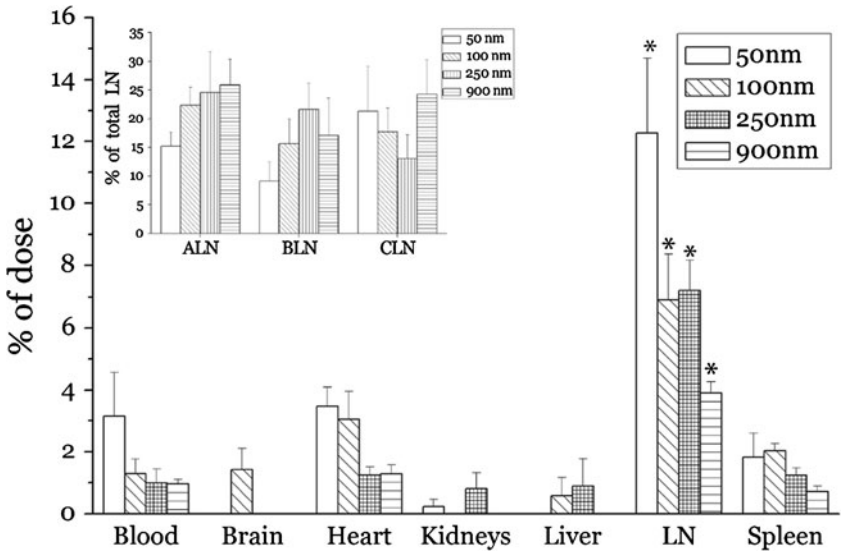

Fig. 5 PN biodistribution 5-hours after pulmonary administration as a % of dose. LN-Lymph nodes; *,$p < 0.05$ when compared to every tissue among each size ($n=6$; mean ± SEM). Inset; percent PN distribution among various LN. ALN, axillary lymph nodes; BLN, brachial lymph nodes; CLN, cervical lymph nodes.

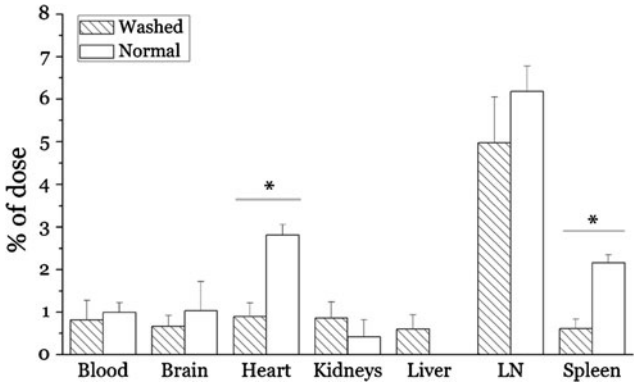

Fig. 6 Biodistribution of PN (normal and washed) of 900 nm size 1 hour after administration to the lungs. LN, lymph nodes; *, $p < 0.05$ between the two data sets ($n=6$; mean ± SEM).

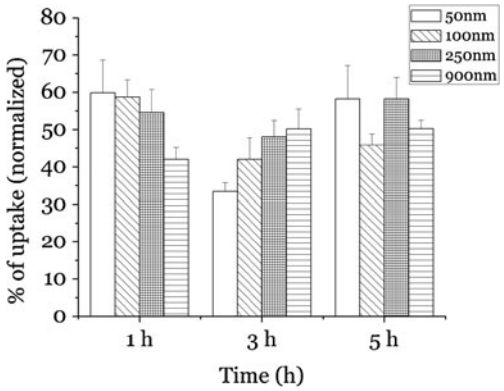

Fig. 8 Normalized lymph node deposition of PN 1, 3, and 5 h after pulmonary administration as a % of uptake ($n=6$; mean ± SEM).

addition, the majority of these studies focused on toxicological aspects of nanoparticle exposures and were designed with this in mind using small administration amounts, multiple exposures extended over time, and primarily utilized histological and qualitative assessments. Pulmonary absorption and biodistribution of PN has been investigated in a single previous study by Sarlo *et al.* (15). In that study, uptake and organ distribution of 20, 100, and 1,000 nm PN administered several times over a period of months was evaluated qualitatively by measurement of an encapsulated dye in organs. It is important to note that the use of a fluorescent dye is an indirect measurement and the presence of the dye itself may alter the uptake and distribution of PN. To evaluate the potential of pulmonary-administered polymeric nanoparticle drug delivery systems for systemic absorption and organ distribution, quantitative, tag-free analysis is required.

Here, we quantitatively investigated the uptake and tissue distribution of 50 nm, 100 nm, 250 nm, and 900 nm diameter PN (as a model polymeric nanoparticle system)

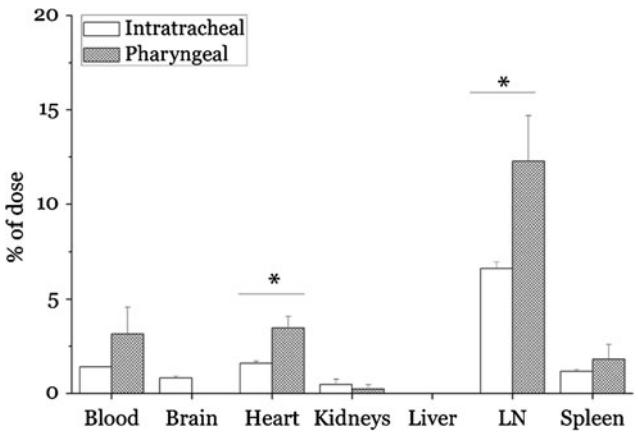

Fig. 7 Comparison of the biodistribution of 50 nm PN 5 h after administration by intratracheal instillation and pharyngeal aspiration. LN, lymph nodes; *, $p < 0.05$ between the two data sets ($n=6$; mean ± SEM).

following pulmonary administration with a tag-free GPC method. We observed that PN of the stated mean diameters distribute from the lungs to LN in relatively large amounts and to other major organs to a lesser extent including little distribution to RES organs. The relatively rapid and high uptake of the non-degradable model PN to LN, in addition to a high LN specificity, suggests potential for LN-directed pulmonary drug delivery with biodegradable nanoparticles of similar characteristics.

The total translocation of PN out of the lungs was found to be significant with as much as 20.9% in as little as 5 h for the 50 nm PN (Fig. 1). The translocation of PN from the lungs to extrapulmonary organs is in accordance with the observations made by Sarlo *et al.*, where they reported the translocation of fluorescently labeled PN of sizes 20, 100, and 1,000 nm diameters from the lungs into various organs including liver, spleen, heart, brain, and kidneys (15). In their study, mice were subjected to an acute exposure or a repeated exposure of fluorescently labeled PN to the lungs followed by qualitative analysis of fluorescent intensities in excised organs. In all cases (the quantitative results presented here and the qualitative observations in the paper by Sarlo *et al.*) the smallest size PN (50 nm and 20 nm, respectively) had the highest extrapulmonary translocation. In addition, at the early time point of 1 h, both studies demonstrate lower uptake for the small PN size compared to larger PN sizes. Size-dependant translocation kinetics, where smaller PN have a relatively slower initial translocation, but higher overall translocation compared to larger PN, may be a result of different internalization pathways. Investigation of lung tissue with TEM demonstrated PN internalization from the alveolar space into the interalveolar septum (Fig. 2). Uptake mechanisms are not directly evident from these images, but are an area of current investigation. PN of 900 nm diameter can be seen within an alveolar macrophage and alveolar epithelium (Fig. 2a), whereas the 50 nm diameter PN are seen in abundant amounts within the epithelium (Fig. 2b). This may indicate disparate mechanisms

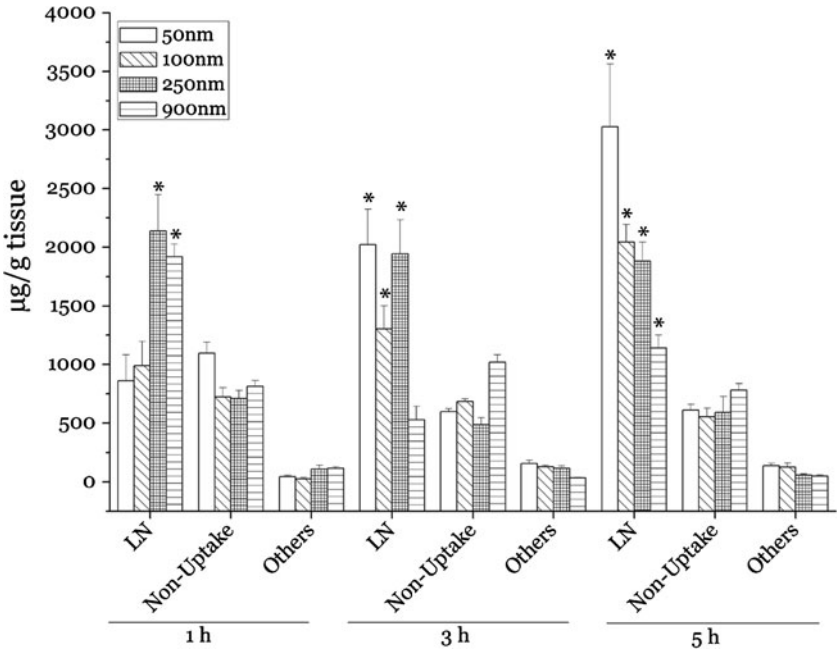

Fig. 9 Lymph node (LN) specificity of PN 1, 3, and 5 h after pulmonary administration. *, $p < 0.05$ when compared to the other two sets of tissues (non-uptake and others) among each size. Amount of PN in LN is represented as $\mu g/g$ of tissue compared to non-uptake (lung, lung rinse, GI) and others (all others including liver, spleen and heart) ($n=6$; mean ± SEM).

of internalization for the two PN sizes and may explain the change in observed size trends in total uptake at 1 h *versus* 3 and 5 h (Fig. 1). For example, the 900 nm PN may have a relatively faster uptake due to macrophage phagocytosis, but over time the 50 nm PN have a higher total uptake potential through the abundant caveolar pits of the alveolar epithelium. Further work is needed to validate these hypotheses; however, it is clear that PN of all sizes are being internalized from the lung alveoli as indicated from our quantitative uptake and biodistribution analysis.

Following translocation from the lung, the tissue of highest PN deposition is the LN. The amount of 50 nm PN in LN is 12.3% at 5 h, which is more than half the total uptake (20.9%). This is a particularly significant amount of lymph node translocation of PN in a short time frame of 5 h. Histological examination of the ALN resulted in discrete irregular aggregates of PN that are distinct from the surrounding nuclei as represented in Fig. 10. The irregular aggregated pattern does not resemble any immune cells of the lymph nodes or any other structure belonging to lymph nodes. Therefore, it can be said that the aggregate we observe in the ALN is likely to be a group of PN. Further, we postulate that the PN transit to the LN by route of macrophage or dendritic cell transit due to the aggregated nature of the PN in the ALN. However, the mechanism of transit remains elusive and is a current focus of the authors.

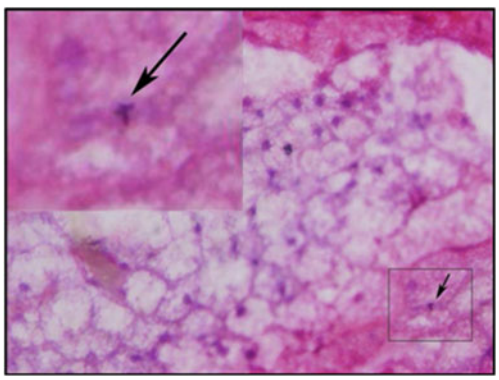

Fig. 10 Histological image of the axillary lymph node (ALN) 5 h after pulmonary administration of 250 nm PN (630X magnification). Inset; digital magnification of the cluster of PN (arrow) in the ALN. PN cluster is distinct from the bigger and more regular shaped nuclei seen throughout the image.

Previously, it was shown that polymer nanoparticles of different sizes and surface properties passively deposit in the lymph nodes (popliteal, iliac, inguinal, and renal lymph nodes) when administered under the dorsal surface of the left hind footpad in rats (16). However, subcutaneous or intramuscular injection routes of administration have not been shown to effectively target nanoparticles to the regional lymph nodes of the thoracic cavity and neck (i.e. ALN, BLN, and CLN), which play a critical role in many diseases including breast cancer, lung cancer, and lymphadenopathies. Oussoren and Storm have shown that liposomes of 100 nm size do deposit in ALN and BLN, but at a very low amount (of less than 2% of injected dose/g of tissue) following subcutaneous administration (17). In contrast to this, we see a very high amount of PN depositing to the ALN, BLN and CLN after pulmonary administration, ranging from 90-230% of administered dose/g of tissue (when calculated in the same manner as Oussoren and Storm). This suggests that pulmonary administration may be a preferred route to effectively deposit nanoparticles in the ALN and BLN.

An interesting observation from the LN deposition of PN is that, though the 50 nm PN had the highest LN deposition (Fig. 5), the 900 nm PN had a greater percent of the

absorbed PN depositing in LN (Fig. 8). This is an important observation indicating the greater fraction of the absorbed PN accumulating in the LN presents a potential for effective LN targeting, thereby significantly reducing the possibility of systemic side effects. Moreover, PN of all the sizes tested have a higher propensity to deposit in the LN as compared to other tissues.

The specificity of PN for LN over major organs, especially the RES organs (liver and spleen), is a remarkable result. From Fig. 9, at the 5 h time point the amount of PN in LN is in the range of 1,140–3,027 μg /g of tissue with the highest deposition being for the 50 nm size, and lowest for the 900 nm size. Considering the small size and weight of the LN, this is a significant amount of deposition and may indicate localized therapeutic potential for biodegradable nanocarriers of similar properties to the model PN. Therefore, the significant amount of uptake from lungs in the short time period of 5 h in addition to the high propensity of PN distribution to the LN uncovers the potential of nanoparticulate pulmonary drug delivery systems for systemic and lymph-targeted therapies.

The liver, spleen, and lungs constitute the RES, which is responsible in removing foreign substances from blood circulation following opsonization (18). When administered intravenously, a great majority of polymer nanoparticles accumulate in the liver and spleen as a result of RES sequestration (15,19–23). Evasion of RES has become a large area of interest in the drug delivery field resulting in the prevalence of 'stealth', PEGylated carrier systems. It has been widely reported that a great proportion of polymeric and non-polymeric nanoparticles are sequestered by the RES within a time frame of minutes to less than an hour after intravenous administration (24–26). However, when administered to the lungs, we show that the PN are deposited in small amounts (of less than 2% of administered dose) in the liver and spleen. This result is in accordance with the observation by Sarlo *et al.* (15), where less than 1% of the recovered dose of fluorescently labeled PN was deposited in the liver and spleen following administration to lungs by pharyngeal aspiration. The small amount of deposition in liver and spleen could be as a result of primary deposition happening in the lymph nodes from where a secondary transit in small amounts into systemic circulation might occur. The negligible amounts of PN deposited in the liver and spleen is of particular interest as it indicates the pulmonary route as another potential systemic delivery mechanism to evade RES.

PN that do distribute to the RES organs are found mostly in the spleen and the biodistribution pattern of spleen mimics the general trend of biodistribution in LN. At the 1-hour time point in spleen, we see a general trend of increase in the amount of PN with increasing size as seen in LN (Fig. 3). However, at 3 and 5 h, we see the amount of PN in spleen decreases with an increase in size, again similar to LN at these time points (Figs. 4 and 5). We speculate that PN transit from the lung to LN, and then through the lymphatic system to the spleen. This is further substantiated by the observation of PN in higher amounts in the spleen than liver. If PN transit to the spleen were to occur through the blood circulation, we would expect to see deposition in both the liver and spleen by RES sequestration.

In order to further verify the observed biodistribution data, 50 nm PN uptake and distribution studies (the study group with highest total uptake and lymph distribution) were repeated under additional study conditions. To ensure that the suspension medium was not a factor influencing total uptake, PN were washed several times, lyophilized and resuspended by probe and bath sonication in sterile, normal saline. Size characterizations of the washed and commercial suspensions by DLS were not statistically different (Table I). Uptake and biodistribution results from the washed nanoparticle study group were similar to the studies discussed above, with the exception of statistically lower distribution in the heart and spleen (Fig. 6). Distribution to the organ with highest distribution, LN, was lower, but not statistically significant. Therefore, the observed study results are unlikely to be an effect of suspension media. Additionally, we repeated studies using intratracheal installation despite pharyngeal aspiration already being validated by other labs (12,15), and found very similar results, but with a slight, statistically insignificant decrease in the total uptake. There were statistically significant differences in the two organs of highest distribution, LN and heart, with the intratracheal administration having lower deposition in those organs (Fig. 7). This decrease in uptake may be due to non-even lung deposition (i.e. deposition into a single lobe) common with intratracheal administration (12). Histology of the lung following PN administration demonstrates that the alveolar wall was of normal thickness and there was no evidence of alveolar collapse. In the lung (Fig. 1 inset), there appears to be little or no severe cell infiltration and inflammation, suggesting that the PN administration caused no severe acute damage to the lungs. In contrast, the intratracheal instillation technique of administering the payload to lungs invokes severe cell infiltration and inflammation due to invasiveness of the technique (27). Therefore, we feel the pharyngeal aspiration technique is more suitable for studying the biodistribution of nanoparticles from lungs. Recently, the method has gained attention as a more suitable technique for studying chemically induced diseases such as asthma (28).

The quantitative nature of the GPC assay used allowed us to determine mass balance for all study groups. The mass balance of PN ranges from 80–90% of the administered dose for all sizes at 1 h. However, it decreases with time for all sizes (Supplementary Material Figure S2). We attribute this decrease in mass balance to the possible redistribution of PN to

tissues like muscle, bone, adipose tissue, urine, etc.: tissues that were not collected in this study. In the discussion above we took the conservative approach of only considering the particles detected in tissues when calculating uptake. However, our mass balance indicates that the potential uptake may actually be higher. Supplementary Material Figure S3 represents the amount of PN in the lungs at all time points for all PN sizes. Except for the 900 nm PN, there is a general trend of decrease in the PN amounts in lungs with time.

CONCLUSION

This study illustrates the potential of nanoparticles administered to the lungs for systemic use in general, and lymph related therapies in particular. Though clear differences in biodistribution and uptake were observed based on the nanoparticle size, other physiochemical parameters also affect the biodistribution, but are not in the scope of this work. The relationship between organ distribution and nanoparticle properties is a complex problem and we have taken a systematic approach to understand a single parameter, nanoparticle diameter, on distribution following pulmonary administration. Further systematic work is needed to evaluate other parameters such as surface chemistry, hydrophilicity, surface morphology, shape and density. Additionally, we evaluated a model polymer nanoparticle system here and translation of observations to a viable, biodegradable polymer nanoparticle system is a current focus. Furthermore, when designing nanoparticles for pulmonary administration, the potential of toxicity to the lungs needs to be taken into consideration.

We observed a higher deposition of nanoparticles in the regional lymph nodes as compared to other major tissues such as RES tissues. The importance of this result is augmented by the relatively rapid transit following lung administration ($\leq$5 h). Further research in this area is needed to exploit the potential of nanoparticles delivered via oral inhalation for vaccines or in the treatment of an array of lymph related disorders.

ACKNOWLEDGMENTS AND DISCLOSURES

This work was supported by the Department of Pharmaceutical Sciences, Eugene Applebaum College of Pharmacy and Health Sciences, and the Office of the Vice President for Research, Wayne State University. We thank Professors David Oupicky, James Granneman and John Reiner at Wayne State University for giving us access to their laboratory equipment, in particular, DLS, TEM, and the light microscope. We also thank Professor Sandro da Rocha, Wayne State University, for proofreading the manuscript. Cubist Pharmaceutical, Inc. has funded unrelated research projects in the laboratory of the corresponding author, JJR. No other potential conflicts of interest exist.

REFERENCES

1. Smola M, Vandamme T, Sokolowski A. Nanocarriers as pulmonary drug delivery systems to treat and to diagnose respiratory and non respiratory diseases. Int J Nanomedicine. 2008;3(1):1–19.
2. Patton JS. Mechanisms of macromolecule absorption by the lungs. Adv Drug Deliv Rev. 1996;19(1):3–36.
3. Sung JC, Pulliam BL, Edwards DA. Nanoparticles for drug delivery to the lungs. Trends Biotechnol. 2007;25(12):563–70. Epub 2007/11/13.
4. Patel LN, Wang J, Kim KJ, Borok Z, Crandall ED, Shen WC. Conjugation with cationic cell-penetrating peptide increases pulmonary absorption of insulin. Mol Pharm. 2009;6(2):492–503. Epub 2009/02/21.
5. Koushik K, Dhanda DS, Cheruvu NP, Kompella UB. Pulmonary delivery of deslorelin: large-porous PLGA particles and HPbetaCD complexes. Pharm Res. 2004;21(7):1119–26. Epub 2004/08/05.
6. Lee J, Oh YJ, Lee SK, Lee KY. Facile control of porous structures of polymer microspheres using an osmotic agent for pulmonary delivery. J Control Release. 2010;146(1):61–7.
7. Zhang Q, Shen Z, Nagai T. Prolonged hypoglycemic effect of insulin-loaded polybutylcyanoacrylate nanoparticles after pulmonary administration to normal rats. Int J Pharm. 2001;218(1–2):75–80. Epub 2001/05/05.
8. Kawashima Y, Yamamoto H, Takeuchi H, Fujioka S, Hino T. Pulmonary delivery of insulin with nebulized DL-lactide/glycolide copolymer (PLGA) nanospheres to prolong hypoglycemic effect. J Control Release. 1999;62(1–2):279–87. Epub 1999/10/16.
9. Choi HS, Ashitate Y, Lee JH, Kim SH, Matsui A, Insin N, *et al.* Rapid translocation of nanoparticles from the lung airspaces to the body. Nat Biotechnol. 2010;28(12):1300–3. Epub 2010/11/09.
10. Korn ED, Weisman RA. Phagocytosis of latex beads by Acanthamoeba. II. Electron microscopic study of the initial events. J Cell Biol. 1967;34(1):219–27. Epub 1967/07/01.
11. Rejman J, Oberle V, Zuhorn IS, Hoekstra D. Size-dependent internalization of particles via the pathways of clathrin- and caveolae-mediated endocytosis. Biochem J. 2004;377(Pt 1):159–69. Epub 2003/09/25.
12. Rao GV, Tinkle S, Weissman DN, Antonini JM, Kashon ML, Salmen R, *et al.* Efficacy of a technique for exposing the mouse lung to particles aspirated from the pharynx. J Toxicol Environ Health A. 2003;66(15):1441–52. Epub 2003/07/15.
13. Florence AT, Hillery AM, Hussain N, Jani PU. Nanoparticles as carriers for oral peptide absorption: studies on particle uptake and fate. J Control Release. 1995;36(1–2):39–46.
14. Jani P, Halbert GW, Langridge J, Florence AT. Nanoparticle uptake by the rat gastrointestinal mucosa: quantitation and particle size dependency. J Pharm Pharmacol. 1990;42(12):821–6. Epub 1990/12/01.
15. Sarlo K, Blackburn KL, Clark ED, Grothaus J, Chaney J, Neu S, *et al.* Tissue distribution of 20 nm, 100 nm and 1000 nm fluorescent polystyrene latex nanospheres following acute systemic or acute and repeat airway exposure in the rat. Toxicology. 2009;263(2–3):117–26.
16. Rao DA, Robinson JR. Effect of size and surface properties of biodegradable PLGA-PMA: PLA:PEG nanoparticles on lymphatic uptake and retention in rats. J Control Release. 2008;132(3):e45–7.
17. Oussoren C, Storm G. Targeting to lymph nodes by subcutaneous administration of liposomes. Int J Pharm. 1998;162(1–2):39–44.
18. Saxena V, Sadoqi M, Shao J. Polymeric nanoparticulate delivery system for Indocyanine green: biodistribution in healthy mice. Int J Pharm. 2006;308(1–2):200–4. Epub 2006/01/03.
19. Yaseen MA, Yu J, Jung B, Wong MS, Anvari B. Biodistribution of encapsulated indocyanine green in healthy mice. Mol Pharm. 2009;6(5):1321–32. Epub 2009/10/06.

20. Shan X, Liu C, Yuan Y, Xu F, Tao X, Sheng Y, *et al.* In vitro macrophage uptake and in vivo biodistribution of long-circulation nanoparticles with poly(ethylene-glycol)-modified PLA (BAB type) triblock copolymer. Colloids Surf B Biointerfaces. 2009;72 (2):303–11. Epub 2009/05/20.
21. Bazile DV, Ropert C, Huve P, Verrecchia T, Marlard M, Frydman A, *et al.* Body distribution of fully biodegradable [14C]-poly(lactic acid) nanoparticles coated with albumin after parenteral administration to rats. Biomaterials. 1992;13(15):1093–102. Epub 1992/01/01.
22. Simon BH, Ando HY, Gupta PK. Circulation time and body distribution of 14C-labeled amino-modified polystyrene nanoparticles in mice. J Pharm Sci. 1995;84(10):1249–53. Epub 1995/10/01.
23. Panagi Z, Beletsi A, Evangelatos G, Livaniou E, Ithakissios DS, Avgoustakis K. Effect of dose on the biodistribution and pharmacokinetics of PLGA and PLGA-mPEG nanoparticles. Int J Pharm. 2001;221(1–2):143–52. Epub 2001/06/09.
24. Gref R, Domb A, Quellec P, Blunk T, Müller RH, Verbavatz JM, *et al.* The controlled intravenous delivery of drugs using PEG-coated sterically stabilized nanospheres. Adv Drug Deliv Rev. 1995;16(2–3):215–33.
25. Illum L, Davis SS, Muller RH, Mak E, West P. The organ distribution and circulation time of intravenously injected colloidal carriers sterically stabilized with a block copolymer–poloxamine 908. Life Sci. 1987;40(4):367–74. Epub 1987/01/26.
26. Sadauskas E, Wallin H, Stoltenberg M, Vogel U, Doering P, Larsen A, *et al.* Kupffer cells are central in the removal of nanoparticles from the organism. Part Fibre Toxicol. 2007;4:10. Epub 2007/10/24.
27. Zhang LJ, Xing B, Wu J, Xu B, Fang XL. Biodistribution in mice and severity of damage in rat lungs following pulmonary delivery of 9-nitrocamptothecin liposomes. Pulm Pharmacol Ther. 2008;21 (1):239–46. Epub 2007/06/15.
28. De Vooght V, Vanoirbeek JA, Haenen S, Verbeken E, Nemery B, Hoet PH. Oropharyngeal aspiration: an alternative route for challenging in a mouse model of chemical-induced asthma. Toxicology. 2009;259(1–2):84–9. Epub 2009/05/12.